Combustion and Flame 161 (2014) 1432–1443

Contents lists available at ScienceDirect

Combustion and Flame

journal homepage: www.elsevier.com/locate/combustflame

Ignition delay times, laminar flame speeds, and mechanism validation for natural gas/hydrogen blends at elevated pressures

Nicola Donohoe [a], Alexander Heufer [a], Wayne K. Metcalfe [a], Henry J. Curran [a,*], Marissa L. Davis [b], Olivier Mathieu [b], Drew Plichta [b], Anibal Morones [b], Eric L. Petersen [b], Felix Güthe [c]

[a] National University of Ireland, Galway, Ireland
[b] Texas A&M University, College Station, TX, USA
[c] Alstom, Baden, Switzerland

ARTICLE INFO

Article history:
Received 28 August 2013
Received in revised form 13 November 2013
Accepted 3 December 2013
Available online 30 December 2013

Keywords:
Hydrogen
Natural gas
Rapid compression machine
Shock tube
Flame speed

ABSTRACT

New experimental ignition delay time data measured in both a shock tube and in a rapid compression machine were taken to determine the increase in reactivity due to the addition of hydrogen to mixtures of methane and natural gas. Test conditions were determined using a statistical design of experiments approach which allows the experimenter to probe a wide range of variable factors with a comparatively low number of experimental trials. Experiments were performed at 1, 10, and 30 atm in the temperature range 850–1800 K, at equivalence ratios of 0.3, 0.5, and 1.0 and with dilutions ranging from 72% to 90% by volume. Pure methane- and hydrogen-fueled mixtures were prepared in addition to two synthetic 'natural gas'-fueled mixtures comprising methane, ethane, propane, *n*-butane and *n*-pentane, one comprising 81.25/10/5/2.5/1.25% while the other consisted of 62.5/20/10/5/2.5% $C_1/C_2/C_3/C_4/C_5$ components to encompass a wide range of possible natural gas compositions. A heated, constant-volume combustion vessel was also utilized to experimentally determine laminar flame speed for the same baseline range of fuels. In this test, a parametric sweep of equivalence ratio, 0.7–1.3, was conducted at each condition, and the hydrogen content was varied from 50% to 90% by volume. The initial temperature and pressure varied from 300 to 450 K and 1 to 5 atm, respectively. Flame speed experiments conducted above atmospheric pressure utilized a 1:6 oxygen-to-helium ratio to curb the hydrodynamic and thermal instabilities that arise when conducting laminar flame speed experiments. All experiments were simulated using a detailed chemical kinetic model. Overall good agreement is observed between the simulations and the experimental results. A discussion of the important reactions promoting and inhibiting reactivity is included.

1. Introduction

Fuel flexibility, increasing efficiency, and reduction in harmful emissions pose ever increasing challenges to the power generation industry. Due to increasing energy costs, dwindling traditional feedstocks and the simultaneous demand for cleaner energy in a power generation market competitive for efficiency and flexibility, the importance of alternative fuels sources is increasing. Energy sources such as coal gas, gases from industrial processes like coke manufacturing, biomass gasification and energy storage via hydrogen electrolysis have become potential alternative energy sources for the gas turbine industry. These gases are typically comprised of hydrogen, syngas (H_2/CO mixtures), and short-chain hydrocarbons generally classified as natural gas. Interest in hydrogen as a renewable energy source for use in gas turbines, fuel cells, and as a transportation fuel has increased in recent years, as it is considered energy dense (on a mass basis) and environmentally friendly.

New routes to hydrogen formation have also led to increased attention; these include steam reformation of hydrocarbons, hydrogen generation via electrolysis of water, and coal/biomass gasification. A growing number of technologies are now harnessing the power of hydrogen to achieve the objective of reducing emissions and increasing fuel flexibility, including integrated gasification combined cycle power plants with carbon capture and storage and I.C. engines. All of this technological progress has made hydrogen fuel particularly interesting to the gas turbine industry. While operating gas turbines with pure hydrogen fuels poses some difficulties and requires significantly re-designed combustion systems and turbomachinery, the addition of hydrogen to natural gas mixtures is expected to alter the combustion properties only slightly [1], leading to a reduction in carbon monoxide, carbon dioxide and NO_x emissions from power generation gas turbine plants.

Even though natural gas is being widely used in the gas turbine industry, it does have some unfavorable combustion characteristics,

* Corresponding author. Fax: +353 91 525700.
E-mail address: henry.curran@nuigalway.ie (H.J. Curran).

0010-2180/$ - see front matter © 2013 The Combustion Institute. Published by Elsevier Inc. All rights reserved.
http://dx.doi.org/10.1016/j.combustflame.2013.12.005

such as a high flammability limit on the lean side and generally low reactivity which limits the operability to richer regimes. These limitations can be improved by the addition of hydrogen which can significantly lower the flammability limit of natural gas mixtures and extend the operability of natural gas turbines to leaner burning regimes [2]. Hydrogen can be mixed with natural gas and/or methane in concentrations of up to approximately 70% to assist the complete combustion of mixtures and reduce emissions. Previous studies have shown that, at up to approximately 50% hydrogen content by volume, the effect on fuel behavior is slight [1,3].

To implement mixtures of these fuels in gas turbines, detailed chemical kinetic mechanisms describing their combustion properties must be developed and validated against a wide range of experimental data for use in design-relevant simulations. In this study, a rapid compression machine (RCM), shock tube, and spherical flame have been employed to study the oxidation of natural gas/hydrogen blends over gas turbine-relevant conditions. Two natural gas mixtures have been studied to better reflect the varying composition of natural gas blends containing greater amounts of higher-order hydrocarbons derived from sources such as coal used in the power generation industry. The study of quinternary natural gas mixtures reflects better the real natural gas blends used in the gas turbine industry as opposed to their single- and binary-component counterparts, which have traditionally been utilized as natural gas surrogates.

Natural gas blends of interest to the gas turbine industry have been characterized previously. Healy et al. [4–9] studied quinternary natural gas mixtures in the temperature range 630–1550 K, in the pressure range of 10–30 bar and developed a detailed chemical kinetic mechanism for natural gas mixtures. Natural gas/hydrogen blends have also come under investigation recently. Park et al. [10] observed a reduction in reactivity when hydrocarbons such as propane or *n*-butane replaced methane in hydrogen/methane and syngas/methane flame mixtures. This reactivity reduction was determined to be a result of the depletion of hydrogen radicals through their consumption in reactions with ethylene (C_2H_4) and ethyl ($\dot{C}_2H_5$) radicals. Reactivity also decreased due to the increased concentrations of methyl ($\dot{C}H_3$) radicals, which consumed further hydrogen atoms through the reactions $CH_4 + \dot{H} = \dot{C}H_3 + H_2$ and $\dot{C}H_3 + \dot{H}(+M) = CH_4(+M)$, lowering the overall rate of the main chain branching reaction $\dot{H} + O_2 = \ddot{O} + \dot{O}H$ [10]. Gersen et al. [11] reported ignition delay times of methane/hydrogen mixtures recorded in a rapid compression machine (RCM) at high pressure (10–70 bar) and intermediate temperature (950–1060 K). They observed that for hydrogen mole fractions above 50% there is a significant decrease in the ignition delay time compared to hydrogen concentrations below 20%, where the effect was slight.

Gersen et al. [11] also observed an increase in global activation energy with higher hydrogen content in the mixture, by reason of the differences in activation energy (Ea) between the two pure fuels, finding that at higher temperatures, the ignition delay time is more greatly reduced by the addition of hydrogen to natural gas mixtures when compared to lower temperatures. Gersen et al. [11] attributed this effect to the increasing importance of the $\dot{H} + O_2 = \ddot{O} + \dot{O}H$ and $H_2 + \dot{O}H = \dot{H} + H_2O$ reactions at higher temperatures. Recently, Gersen et al. [12] expanded their study to include the effect of carbon monoxide on methane, hydrogen, and binary mixtures of the two fuels at high pressures (20–80 bar) and a lean equivalence ratio ($\phi = 0.5$). They found that for $CH_4/H_2/CO$ mixtures there was no inhibiting effect of CO addition compared to binary methane/hydrogen mixtures [12].

Crossley et al. [13] observed the effect of adding ethane, propane, *n*-butane, and *n*-pentane fractions to methane fuel. They determined that the addition of larger hydrocarbons led to a significant reduction in ignition delay time, and this effect was determined to be due to the faster kinetics of the higher hydrocarbon fuels. de Vries and Petersen [14] measured undiluted natural-gas-based mixtures combining methane with ethane, propane, *n*-butane, *n*-pentane, and hydrogen at gas turbine relevant conditions in a shock tube. The results obtained showed a definite decrease in activation energy at lower temperatures and higher pressures as seen in the work of Gersen et al. [11]. Yu et al. [15] and Huang et al. [16] studied methane/hydrogen and propane/hydrogen, and methane/ethane/propane/hydrogen laminar burning velocities, respectively. They determined that an increase in hydrogen mole fraction in any case leads to an increase in laminar burning velocities. Few data have been published on hydrogen/hydrocarbon blend ignition delay times, and to the author's knowledge, no hydrogen/quinternary natural gas blend ignition delay times at gas turbine relevant conditions have been published previously.

While the flame speed of the main component of natural gas, methane, has been extensively studied in the literature [17,18], the laminar flame speeds of methane and natural gas blends with high hydrogen content at elevated temperatures and pressures remains to be studied. Because the flame speed of blended fuels cannot be obtained by linear combination of each blended fuel constituent, modeling work has been done to predict the flame speeds of methane and hydrogen blends by Chen et al. [19]. Correlations for similar fuel blends such as ethane and hydrogen mixtures have been studied by Wu et al. [20]. Flame speeds of butane–air mixtures with hydrogen addition have been experimentally determined in a study by Tang et al. [21], and Yu et al. [15] conducted methane flame speed experiments at atmospheric conditions with a small amount of hydrogen addition. Hu et al. [22] studied the entire range of methane and hydrogen blends at room temperature and pressure. No relevant laminar flame speed data at elevated temperatures and pressures were found in the literature.

As a result of the few fundamental kinetic studies available on methane and natural gas mixtures with hydrogen, the intent of this work was to provide a comprehensive set of ignition delay time and laminar flame speed data over a range of fuel blends at conditions of relevance to gas turbine engines. These data were used to compare with a modern, detailed chemical kinetic mechanism. By combining both RCM and shock-tube capabilities, a wide range of temperatures were examined for the measured ignition delay times. Details of the experimental apparatuses are provided first, namely the RCM, shock-tube, and constant-volume flame speed vessel, followed by an overview of the chemical kinetic mechanism. A comprehensive section detailing the results of the experiments in comparison with the model predictions is then provided. Further mechanism validation against archival data and a detailed sensitivity analysis are then presented.

2. Experimental setup

2.1. NUIG rapid compression machine

Experiments were performed in the rapid compression machine (RCM) facility at the National University of Ireland Galway (NUIG). The NUIG RCM has a horizontally opposed, twin-piston design that has been described in previous studies [23,24]. Compression times below 16 ms are achieved using this set up. The diameter of the reaction chamber is 38.2 mm. The chamber and sleeves are pre-heated to ensure a homogeneous temperature, and this heating can be carried out up to 160 °C. With the addition of creviced pistons, boundary layer effects are negligible, and the reacting core is temperature homogeneous and adiabatic. By varying the initial temperature, initial pressure, diluent gas composition, and volumetric compression ratio a wide temperature range can be investigated.

The ignition delay time (τ) is defined as the time from the end of compression, taken as the time of peak compressed pressure, to the maximum rate of pressure rise at ignition, Fig. 1. To account for the heat losses inherent in RCM experiments, non-reactive experiments are performed in which the oxygen content of the mixture is replaced by nitrogen and then simulated to produce a volume/time history which is used as the input in the Chemkin Pro [25] simulation. Nitrogen is used because it has similar thermodynamic properties to those of oxygen. The recorded pressure profile presents the same pressure drop as a reactive trace as a result of very similar heat loss properties.

Recent experiments in shock tubes and in RCMs have shown that the pressure transducer (Kistler 603B) used in the NUIG facilities is sensitive to heat loads during the experiments. Heat flux from the hot gas into the sensor reduces the output signal so that a lower pressure is measured compared to reality. We have modified our experimental procedure to overcome this problem. The pressure transducer is covered by a thin silicone layer. This layer acts to shield the sensor against the heat load during the experiment. From these experiments, the true experimental compression ratio and pressure profile are determined. We are aware that the use of the silicone layer improves the transducer's measurement characteristics, but the response time of the 603B transducer can be affected by this technique. This effect would manifest itself in times of the order of approximately 1×10^{-5} s. However, in our RCM the measuring times are on the order of milliseconds. Thus, even if one would expect a quite strongly damped natural frequency due to the silicone layer, which one would see by comparing experimental traces with and without silicone, the possible error should be within the usual experimental scatter. In contrast, the effect of the thermal shock is quite significant on the measured pressure and the deduced temperature, see also Mittal and Bhari [26], so that the experimental error would be much more compared to not using a silicone layer.

Since we deduce the temperature profile from the pressure profile via the isentropic relationship, the apparent measured temperature would also be lower compared to reality using the profiles from the non-shielded sensor. This artificially lower temperature would result in longer ignition delay times in the simulation compared to a simulation that used the more-accurate profile measured with the shielded sensor. Furthermore, the temperature at the end of compression would be lower using the end-of-compression pressure of the non-shielded sensor. Thus, this method reduces uncertainties in the temperature of the experiment and simulation. Estimated uncertainty limits of the measurements are ±5 K in compressed gas temperature, ±0.1 bar in compressed gas pressure, ±15% in ignition delay time, τ, and ±2% in mixture composition. All experimental data are provided as Supplementary material.

2.2. Shock tube

Experiments were performed in the large-diameter shock-tube facility described in detail by Aul et al. [27,28]. Made entirely of 304 stainless steel, this shock tube has a driven section that is 4.72 m long with internal diameter of 15.24 cm. The driver section has an internal diameter of 7.62 cm with a length that is 2.46 m. The relatively large diameter of the driven section allows for experiments to be performed with minimal boundary layer effects. Because of the length of the shock tube, ignition delay times of up to 2 ms before any significant pressure drop due to test-ending expansion waves can be observed. For the experiments, either aluminum or polycarbonate diaphragms were used, depending on the desired post-shock pressure. In general, the driver section is filled slowly with helium until the diaphragm bursts to maintain repeatability in breaking pressure and rate of shock formation from test to test.

The conditions at which the combustion event occurs are dictated by the conditions behind the shock wave after it is reflected off the endwall of the driven section of the shock tube. For the shock tube used herein, incident-shock velocity in the test region was found using 5 pressure transducers (PCB 113) connected to 4 time-interval counters (Fluke PM 6666). The velocity of the incident shock wave was found from these counter measurements. Using the standard 1-D shock relations with this velocity, the reflected-shock conditions for each experiment were calculated. Petersen et al. [29] demonstrated that this method determines reflected-shock temperatures that are within 10 K of the actual temperature. Estimated uncertainty limits of the measurements are ±15 K in reflected-shock temperature, T_5, ±15% in ignition delay time, τ, and ±2% in mixture composition. All experimental data are provided as Supplementary material.

In shock-tube experiments with significant energy release, it is ideal to measure the ignition event from the endwall using the endwall pressure signal [30], as depicted in Fig. 2. In the present experiments, the combustion event was exothermic enough in certain mixtures to produce a significant and measurable rise in pressure, such as shown in Fig. 2. Because of the relatively large inner diameter of the shock-tube driven section (15.24 cm),

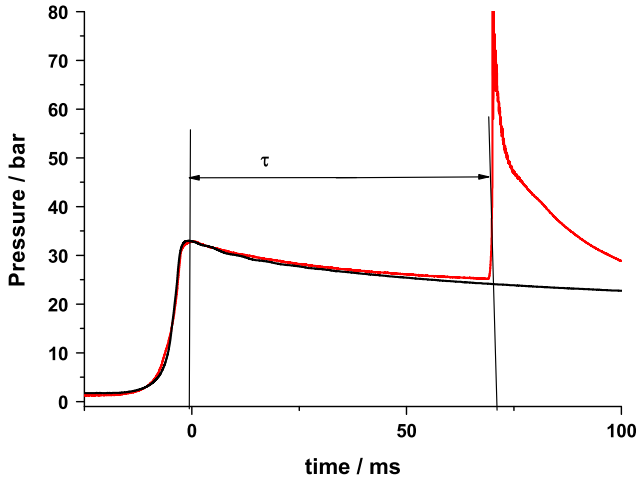

Fig. 1. Sample reactive and non-reactive pressure profiles.

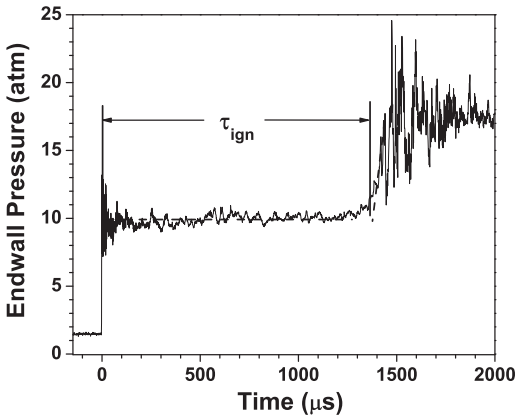

Fig. 2. Ignition delay time measurement from endwall pressure signal. Experiment shown was performed with a mixture of NG3 (see Table 2, defined later) and 30% H_2 with an equivalence ratio of 1 at 9.6 atm and 1199 K. The pressure spike at time zero is due to the vibration of the endwall at arrival of the shock wave and is not indicative of the post-shock gas pressure.

boundary-layer effects on the test conditions were minimal over the range of the experimental results. Typical pressure increases due to the boundary layer, or dp/dt, were on the order of 1.5% per ms (2% worst case). The pressure signal shown in Fig. 2 is indicative of the typical experiment with minimal dp/dt. This level of pressure increase produces a corresponding temperature increase of about 7 K after 1 ms.

All shock-tube mixtures herein were diluted in 90% argon and, due to this moderate dilution level, some of the mixtures used were not exothermic enough at all conditions to produce a strong pressure rise at the endwall, such as that seen in Fig. 2. In these few cases, the sidewall OH (A → X) (hereafter referred to as OH*) emission was used to determine the ignition delay time per Petersen [30], as shown in Fig. 3. In such cases, the beginning of the ignition delay time was defined by the sidewall pressure signal, and ignition was indicated by the intersection of the initial OH* concentration (i.e., zero) and the steepest slope of the OH* rise (see Fig. 3).

2.3. Ignition delay time test matrix

The effect of hydrogen addition to methane and natural gas has been shown to vary with the amount of higher-order hydrocarbons in the natural gas, the equivalence ratio (ϕ), and the pressure [31,32]. However, putting together a test list covering a wide range of pressures, % hydrogen, stoichiometry, and fuel blend could prove a huge task due to the large number of possible combinations. A test matrix was therefore developed to test these different properties in an organized yet efficient manner. Three levels of each variable were assembled into an L9 Taguchi array [33], shown in Table 1. The specific mole fractions for the NG2 and NG3 blends are provided in Table 2. These two fuel blends have been used quite extensively by the authors in previous work and are representative of the range of natural gases containing moderate (NG2) and high (NG3) levels of higher-order hydrocarbons [34,8,1]. The four independent variables selected were fuel (CH_4, NG2, NG3); $\%H_2$ in the fuel (30, 60, 80 by volume); the equivalence ratio (0.3, 0.5, 1.0); and the target pressure (1, 10, 30 atm). The temperature was changed for each matrix combination to cover the entire possible range for each mixture; the temperature ranges varied to obtain ignition delay times from around 100 μs to 200 ms. Therefore, temperature was not included specifically in the test matrix. Tables of data recorded in both the RCM and in the shock tube are provided in the Supplementary material.

Ultra-high purity (UHP, 99.9995%) gases were used to make the test mixtures. The two natural gases used in the study were each prepared separately from the main fuel–O_2–diluent mixtures to ensure repeatability with the natural gases used. The natural gases were prepared using the partial pressure method in tanks that were initially evacuated. The partial pressure of pentane was kept well below the saturated vapor pressure of the fuel to ensure that it remained in the gaseous phase and was well incorporated in the natural gas mixtures. After the natural gas mixtures were prepared, the mixtures from the test matrix were made. All mixtures from the main L9 matrix were diluted in 90% diluent by volume. For the shock-tube measurements, the diluent used was argon, while a 50/50 mixture of argon and nitrogen was used for the RCM experiments. Fuel in 'air' experiments were also performed in the RCM to determine the effect of dilution on the mixtures as detailed in Table 1.

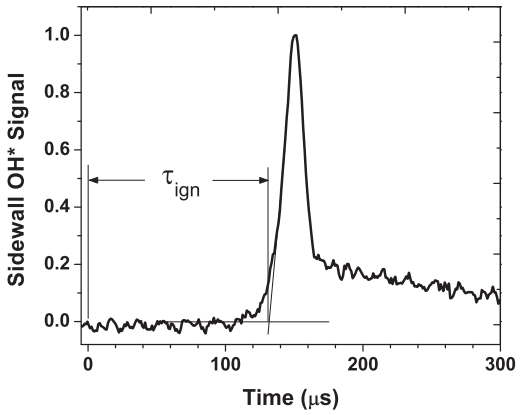

Fig. 3. Ignition delay time measurement from the sidewall OH* emission signal, for a case where the ignition event was not evident in the pressure rise. The experiment shown was performed in a mixture of CH_4 and 30% H_2 with an equivalence ratio of 0.3 at conditions of 1.5 atm and 1645 K.

Table 1
Mixtures studied, chosen using the Taguchi method for balanced, orthogonal arrays [33]. Three levels of each factor were used. Mixtures 2b, 3b, 4b, and 6b are fuel mixtures diluted in 'air'. The values under the fuels represent mole fractions.

Mix	CH_4	H_2	O_2	Diluent	ϕ	% H_2	p
1	0.01135	0.00486	0.08378	0.9	0.3	30	1
2	0.0125	0.01875	0.06875	0.9	0.5	60	10
2b	0.0348	0.0523	0.1917	0.7211	0.5	60	10
3	0.01111	0.04444	0.04445	0.9	1.0	80	30
3b	0.0416	0.1663	0.1663	0.6257	1.0	80	30
	NG2						
4	0.0146	0.0063	0.0791	0.9	0.5	30	30
4b	0.0367	0.0158	0.1990	0.7484	0.5	30	30
5	0.0174	0.0261	0.0564	0.9	1.0	60	1
6	0.005	0.02	0.0749	0.9	0.3	80	10
6b	0.0131	0.0524	0.1962	0.7383	0.3	80	10
	NG3						
7	0.0217	0.0093	0.0691	0.9	1.0	30	10
8	0.0067	0.0101	0.0832	0.9	0.3	60	30
9	0.0067	0.0268	0.0666	0.9	0.5	80	1

Table 2
Fuel mixture compositions in percent volume.

Species	CH_4	NG2	NG3
CH_4	100	81.25	62.5
C_2H_6	0.0	10.0	20.0
C_3H_8	0.0	5.0	10.0
n-C_4H_{10}	0.0	2.50	5.0
n-C_5H_{12}	0.0	1.25	2.50

2.4. Laminar flame speed experiments

All laminar flame speed experiments presented in this study were carried out in two different, centrally ignited, constant-volume combustion vessels. The first was a centrally ignited, cylindrical, 7075 aluminum vessel with internal diameter and length of 30.5 cm and 35.6 cm, respectively. The end caps each contained a 6.35-cm thick fused quartz viewing window that when installed allowed for a 12.7-cm viewing port. The combustion event images were captured using a Z-type Schlieren setup with a FastCam SAE 1.1 high-speed camera with a mercury arc lamp as the light source. Further details on this design and experimental methods can be found in the study by de Vries [35] and Lowry et al. [36]. The second vessel is made of 17–4PH stainless steel equipped with a circumferential heating jacket. This heating jacket allows for the elevated initial temperatures in this study of 450 K; it has insulation around the entire vessel to provide temperature uniformity within the vessel. The development and temperature profile are detailed elsewhere in Krejci [37] and Krejci et al. [38]. To view the combustion events on this vessel, a modified Z-type Schlieren setup was utilized as detailed by Plichta et al. [39].

The test matrix for the laminar flame speed tests was determined by varying the fuel, hydrogen content, temperature, and pressure as for the ignition delay time experiments, using methane and NG2 (Table 2) as the primary hydrocarbon fuels. The hydrogen content was varied between 50% and 90% of the fuel mixture by volume. Temperatures of either 300 K or 450 K and pressures of either 1 or 5 atm were utilized. Table 3 summarizes the flame speed matrix for the study herein. Synthetic air was used as the oxidizer for the atmospheric pressure experiments. To curb hydrodynamic and thermal-diffusive instabilities, a 1:6 O_2:He ratio was used as the oxidizer for the 5-atm experiments. This higher diluent-to-oxygen ratio increased flame thickness thereby suppressing hydrodynamic instabilities, and helium's higher diffusivity than nitrogen increased Lewis number, thus decreasing thermal-diffusive instabilities [40]. The 1:6 ratio was specifically chosen to mimic the adiabatic flame temperature of that same fuel with air. A parametric sweep of equivalence ratios was conducted at each condition in Table 3.

The procedure for extracting laminar flame speed is well documented in the literature and therefore will only be briefly discussed here. Constant pressure is one main assumption for the data analysis to find flame speed and is proven by previous studies conducted in the facilities used in this study (see de Vries [35]). The flame radius in this study was also limited to the range where no flame acceleration was detected in order to neglect wall and ignition effects. A post-processing program using the density gradients to track the flame edge used a Taubin circle fit and six-point radius method to find the radius as a function of time as depicted in Fig. 4, which shows flame images from 50/50 CH_4/H_2 and air at standard temperature and pressure. The bottom row shows the detected flame edge with a white line, and fit to that white line are six red points from which the flame radius is extracted. After the change in flame radius over time is determined, corrections need to be made for stretching and to convert to unburned flame speed.

Figure 4 depicts a smooth, laminar flame. As these images were taken from a room-temperature and -pressure experiment, one would expect such a laminar flame. However, these images are representative of all the flame fronts seen in the present study as no turbulent, cellular fronts developed while the flame was propagating throughout the viewing window. Figure 5 shows examples for two cases at the higher pressure of 5 atm. Only large wrinkles were seen to form at 5 atm, but they did not grow and therefore did not affect the flame speed values obtained herein. Hence, the helium dilution for the higher-pressure tests had the desired effect of stabilizing the flame front.

The change in radius (r) over change in time (t) for spherically expanding flames was found by a six-point method. Next, the well-known stretch rate α, Eq. (1), for spherically expanding flames was applied; then the linear method, Eq. (2), was used to extract the un-stretched, burned-gas flame speed, $S^o_{L,b}$. The linear method was chosen because it is accurate to the first order in finding the laminar flame speed and unburned-gas Markstein length, L_m [41]. The latter, along with the constant in Eq. (2), were obtained by linear regression in fitting the experimental $r(t)$ data. The resultant burned flame speed is divided by the unburned-to-burned gas density ratio, σ, to calculate the unburned, un-stretched laminar flame speed, $S^o_{L,u}$, in Eq. (3).

Table 3
Experimental conditions for the laminar flame speed experiments by percentage volume.

Fuel	%H_2	Temperature (K)	Pressure (atm)	Oxidizer
CH_4	50	300	1	Air
CH_4	70	450	5	1:6 O_2:He
NG2	90	300	5	1:6 O_2:He
CH_4	90	450	1	Air

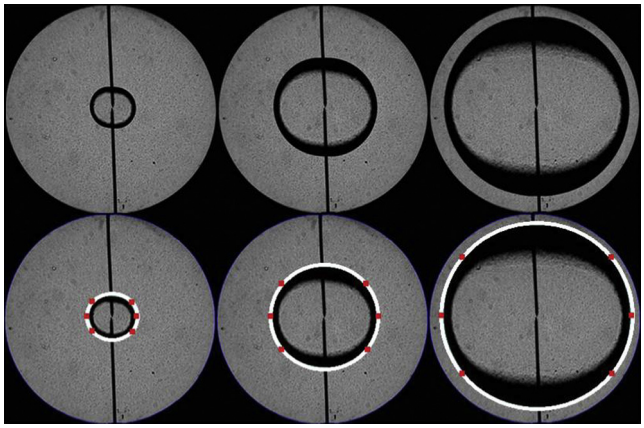

Fig. 4. Captured images (top) and post-processed images (bottom) (50/50 CH_4/H_2 T = 298 K, P = 1 atm). The bottom set shows the edge definition and the 6 points that define the fitted circle.

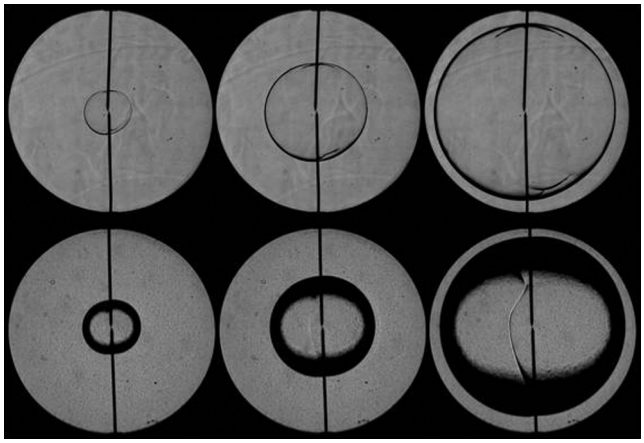

Fig. 5. Typical flame images for the higher pressure of 5 atm. The top set of images are for 30/70 CH_4/H_2, 450 K, 5 atm; the bottom sequence of images is for 10/90 NG2/H_2, 300 K, 5 atm

$$\alpha = \frac{2}{r}\frac{dr}{dt} \tag{1}$$

$$r(t) = S^o_{L,b}t - 2L_m ln(r) + constant \tag{2}$$

$$S^o_{L,u} = \frac{S^o_{L,b}}{\sigma} \tag{3}$$

A rigorous uncertainty analysis was also performed. Using the methods developed by Kline and McClintock [42], the bias and precision uncertainty were coupled to find the total uncertainty. Three main factors contribute to the laminar flame speed uncertainty–temperature (T), pressure (P), and equivalence ratio (ϕ). To find the bias limit, a relationship needed to be developed between these three factors and flame speed. Other places in the literature have developed such correlations by proposing a quadratic function of equivalence ratio with temperature and pressure raised to a constant exponent (e.g., Elia et al. [43]). The present authors have utilized Eq. (4) to find the correlation between all the relevant parameters and flame speed. That is, the flame speed correlation was used only to determine the relationship between the flame speed and the independent parameters (T, P, ϕ) to determine the sensitivities needed to estimate the overall uncertainty, given the uncertainty in each parameter. P_o and T_o represent standard temperature and pressure, 1 atm and 298 K, respectively, and a through j represent fitting constants.

$$S_L(T,P,\phi) = (a + b\phi + c\phi^2 + d\phi^3)\left(\frac{P}{P_o}\right)^{(e+f\phi+g\phi^2)}\left(\frac{T}{T_o}\right)^{(h+i\phi+j\phi^2)} \quad (4)$$

This model of Eq. (4) was applied to each condition, and the constants a through j were determined for each mixture. The temperature dependence in Eq. (4) was ignored for the room-temperature experiments as it became unity. As multiple experiments at each condition and equivalence ratio were not performed, a purely statistical uncertainty could not be determined. However, we have shown in earlier laminar flame speed work that the uncertainty can be well represented by taking the root sum square of the contributions of each parameter to the measured flame speed [35], per the Kline and McClintock method [42]. The sensitivities of S_L with respect to each variable were obtained from the appropriate derivatives of Eq. (4). The uncertainty in ϕ was based on the mixture component partial pressures as measured directly with the pressure transducers located on the mixing manifold. Typical uncertainties in equivalence ratio were less than 2% as mentioned above, and the initial pressure and temperature obtained from the pressure transducer (accuracy of 0.15% of full-scale range) and thermocouple were 0.05 atm and 0.1 K, respectively. Overall, the average uncertainty in the laminar flame speed was about ±8 cm/s, or about 9%. Estimated uncertainties for the range of data are shown as representative error bars in the Results section. Note that the error bars for ϕ are small and would be about the size of the symbols used in the Results section plots and are therefore not shown for clarity.

3. Chemical kinetic mechanism

The chemical kinetic mechanism used in this study, AramcoMech 1.3 [44], has its foundation in the work of Healy et al. [4–9] and was built on the hierarchical nature of hydrocarbon mechanisms with the inclusion of our recently updated hydrogen/carbon monoxide sub-mechanism [45]. In addition, considerable changes have been made to the C_1–C_2 portion of the mechanism which are detailed in the work of Metcalfe et al. [44]. The chemistry of some important unsaturated species including 1,3-butadiene, propene, and allene has been taken from Laskin et al. [46], primarily based on the earlier work of Davis et al. [47]. The C_4 and C_5 sub-mechanisms are taken from the previously mentioned Healy et al. [4–9] studies. All experiments were compared to the current mechanism, AramcoMech 1.3 and for comparison, simulations were also performed using GRI Mech 3.0 [48]. For the natural gas mixtures, the C_4 and C_5 NUIG sub-mechanisms were added as GRI-Mech 3.0 is only validated up to C_3 and this mechanism will hereafter be referred to as the modified GRI-Mech 3.0_M.

For the ignition calculations in a rapid compression machine, a volume profile is generated from the non-reactive pressure trace. These volume histories are used in the Chemkin simulations of our RCM experiments. By doing so we take heat loss during and after compression into account. This approach was first discussed in the work of Mittal et al. [49].

The shock-tube data have been simulated using constant-volume, adiabatic simulation with the reflected-shock pressure and temperature as initial conditions. In the case of the shock-tube data from Zhang et al. [3], our simulations take the 4%/ms pressure rise due to the facility-dependent boundary layer into account as stated by the authors.

The flame speed calculations were performed using the high-temperature C5 version of AramcoMech 1.3, where low-temperature species (peroxy radicals, alkyl hydroperoxides, ketohydroperoxides, etc.) and their reactions are removed. The complete mechanism has 316 species and 1805 reactions, while the high-temperature mechanism contains 188 species and 1273 reactions. The calculations were performed using Chemkin Pro [25]. In our simulations we used the multi-component transport equations, as in a study of syngas mixtures [45] it has been shown that this provides more accurate results compared to mixture-averaged transport models. Simulations were converged to a grid independent solution by assigning GRAD and CURV values of 0.02.

4. Results

Presented in this section are the results from the present experiments along with comparisons with the chemical kinetic model described in the previous section and GRI-Mech 3.0. The RCM and shock-tube results are discussed first, followed by the laminar flame speed results.

4.1. Ignition delay times

Figures 6–8 detail the experimental results obtained in the TAMU shock tube and the NUIG RCM. In all figures, closed symbols represent RCM data, while open symbols represent shock-tube data. The lines are model simulations (AramcoMech 1.3); solid lines correspond to adiabatic, constant volume conditions, while dashed lines include simulations assuming a dp/dt of 2%/ms in the shock-tube experiments. In addition, the dotted lines represent mechanism predictions obtained with GRI-Mech 3.0 [48] in Fig. 6 and GRI-Mech 3.0_M [48] in Figs. 7 and 8. For all conditions, the agreement between the NUIG AramcoMech 1.3 simulation and experiment is quite good and there is only a very small effect of the 2%/ms pressure rise where predicted ignition delay times are slightly faster when compared to the constant volume predictions when times are longer than about 1 ms and are indistinguishable for shorter times.

The trend and effect of hydrogen concentration at all equivalence ratios and pressures are captured by AramcoMech 1.3. This mechanism has previously been validated against RCM ignition delay time measurements for pure hydrogen and syngas mixtures [45] and natural gas [4–9] mixtures taken in the NUIG facility. Over the temperature range (700–1500 K) of these past studies, increasing pressure results in higher reactivity of the mixture and shorter ignition delay times. For the high hydrogen-content fuels, hydrogen chemistry is dominant. In the temperature regime studied, hydrogen reactivity is mainly controlled by the competition between the chain-branching reaction $\dot{H} + O_2 = \dot{O} + \dot{O}H$ and the

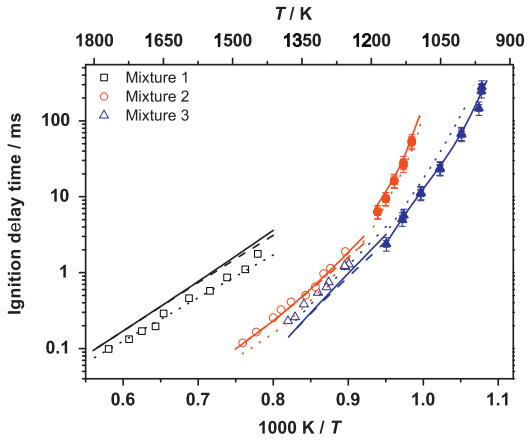

Fig. 6. Ignition delay times of CH_4/H_2 mixtures, □ Mix 1 ST, ○ Mix 2 ST, ● Mix 2 RCM, △ Mix 3 ST, ▲ Mix 3 RCM. Solid lines are AramcoMech 1.3 predictions assuming constant-volume conditions, dashed lines are AramcoMech 1.3 predictions assuming a dp/dt of 2%/ms in the shock-tube experiments and dotted lines are GRI-Mech 3.0 predictions.

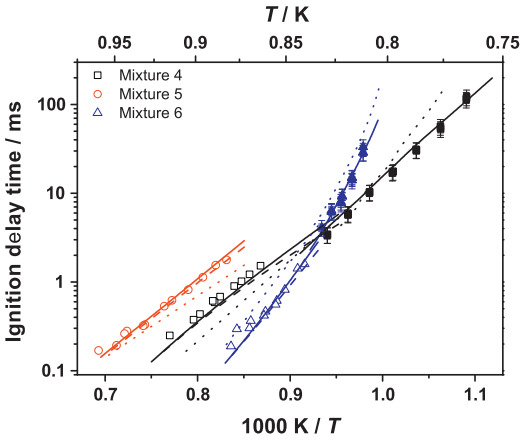

Fig. 7. Ignition delay times of NG2/H_2 mixtures, □ Mix 4 ST, ■ Mix 4 RCM, ○ Mix 5 ST, △ Mix 6 ST, ▲ Mix 6 RCM. Solid lines are AramcoMech 1.3 predictions assuming constant-volume conditions, dashed lines are AramcoMech 1.3 predictions assuming a dp/dt of 2%/ms in the shock-tube experiments and dotted lines are GRI-Mech 3.0_M predictions.

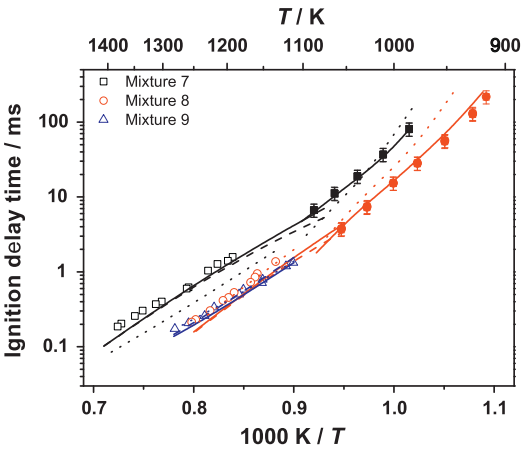

Fig. 8. Ignition delay times of NG3/H_2 mixtures, □ Mix 7 ST, ■ Mix 7 RCM, ○ Mix 8 ST, ● Mix 8 RCM, △ Mix 9 ST. Solid lines are AramcoMech 1.3 predictions assuming constant-volume conditions, dashed lines are AramcoMech 1.3 predictions assuming a dp/dt of 2%/ms in the shock-tube experiments and dotted lines are GRI-Mech 3.0_M predictions.

pressure-dependent, chain-propagating reaction $\dot{H} + O_2(+M) = H\dot{O}_2(+M)$ leading to a cross over in reactivity at higher temperatures, as can be seen in Fig. 7. In hydrocarbon fuels, low-temperature alkane chemistry and alkyl radical reactions with hydroperoxyl radicals, particularly the reaction $RH + H\dot{O}_2 = \dot{R} + H_2O_2$ followed by hydrogen peroxide decomposition, $H_2O_2(+M) = \dot{O}H + \dot{O}H(+M)$, control the reactivity as described previously by Healy et al. [8]. The low temperature ignition delays are accurately modeled by the current mechanism.

The shock-tube ignition delay experiments, whose chemistry is governed by the reaction $\dot{H} + O_2 = \ddot{O} + \dot{O}H$ and the concentration of oxygen in the system, agree well with those taken in the RCM. In addition, the effect of adding higher hydrocarbons and the effect of increasing higher hydrocarbon content is demonstrated precisely, Figs. 6–8. The agreement between shock tube and RCM is quite good, and the facility effects exhibited by both machines are accurately captured by the present modeling procedure. In Fig. 6, mixture 3 shows the highest reactivity, with mixture 1 exhibiting the slowest reactivity. The reason for the observed increase in reactivity of mixture 3 is due primarily to the high hydrogen mole fraction and pressure of the mixture (80% H_2, ϕ = 1.0, 30 atm) compared to mixture 1 (30% H_2, ϕ = 0.3, 1 atm). The same is true of Figs. 7 and 8 with the NG2 and NG3 mixtures containing the largest hydrogen mole fractions exhibiting the highest reactivity over all conditions studied.

For methane/hydrogen mixtures, Fig. 6, GRI-Mech 3.0 does not accurately reproduce the RCM or the shock-tube results obtained in this study except for mixtures 1 and 3 for the shock-tube conditions. For the NG2/hydrogen, Fig. 7 and NG3/hydrogen mixtures, Fig. 8, AramcoMech 1.3 performs better for both the RCM and shock-tube experiments than GRI-Mech 3.0_M except for the shock-tube data of mixture 8. AramcoMech 1.3 slightly overpredicts the ignition delay time for mixture 1 in Fig. 6. There is a discrepancy between the mechanism predictions of GRI-Mech 3.0_M and the experimental data. This difference can possibly be explained by the fact that GRI-Mech 3.0 has a tendency to overpredict ignition delay times for hydrogen and under predict hydrocarbon ignition delay times compared to AramcoMech 1.3 and also because the latter mechanism was designed with higher-pressure and lower-temperature ignition data in mind. Overall AramcoMech 1.3 performs well compared to the experimental ignition delay time data presented here.

Figure 9 illustrates the effect of dilution on experiments taken in the NUIG RCM. Closed symbols represent fuel/air experiments, open symbols diluted data, and lines are model simulations. Solid lines correspond to closed symbols and dashed lines to open symbols using AramcoMech 1.3, while the dash dot and dotted line represents the GRI-Mech 3.0_M simulations [48]. For all of the mixtures, dilution leads to lower reactivity and longer ignition delay times, as there is less fuel and oxygen in the mixture. The trends for both the non-diluted and diluted experiments are captured very well by AramcoMech 1.3. GRI-Mech 3.0_M however, generally predicts longer ignition times compared to those measured experimentally, and it does not well-reproduce the activation energy for the fuel-in-air mixtures, where the temperature dependence is predicted to be stronger compared to that measured experimentally. Further comparisons of model predictions versus our experimental data are provided in Fig. 1 of the Supplementary material.

4.2. Laminar flame speeds

To start the discussion of the laminar flame speed results, it is worthwhile to contrast the cases for pure CH_4 (lowest S_L) and pure H_2 (highest S_L) with a typical H_2/CH_4 blend composing a 50/50

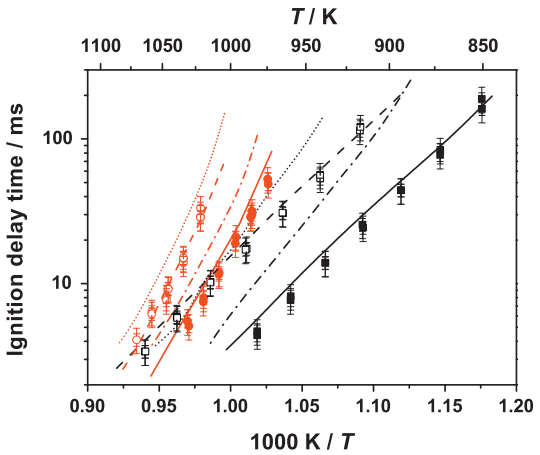

Fig. 9. Effect of dilution on ignition delay times of NG2/H_2 mixtures in NUIG RCM, □ Mix 4 diluted ■ Mix 4 fuel-in-air, ○ Mix 6 diluted, ● Mix 6 fuel-in-air. Solid and dashed lines are AramcoMech 1.3 predictions, and dash dot and dotted lines are GRI-Mech 3.0_M predictions for undiluted and diluted mixtures, respectively.

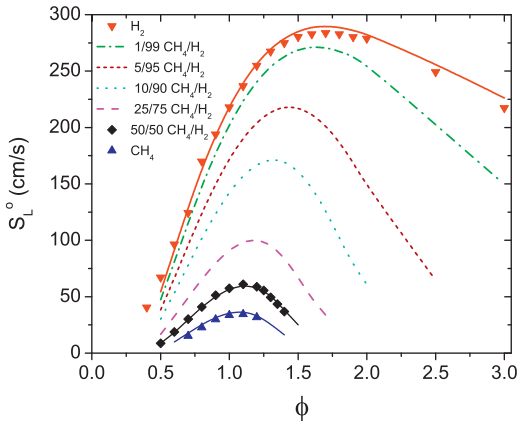

Fig. 10. Laminar flame speed comparison of pure and blended CH_4 and H_2 at various equivalence ratios at 300 K and 1 atm in air, in contrast to where a 50/50 blend of the two fuels resides. Points are experimental data, and lines are from the kinetics model. The 50/50 blend results are from the present study, while the CH_4 data are from Lowry et al. [36], and the H_2 data are from Krejci et al. [38].

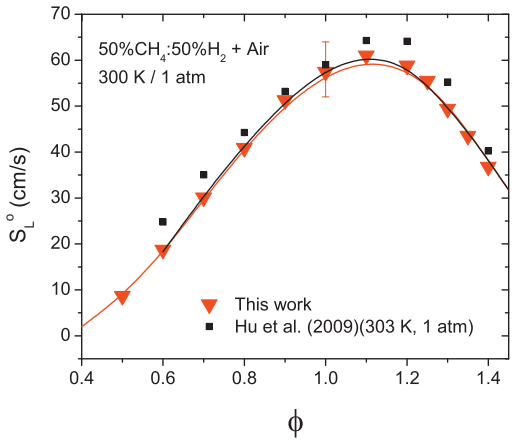

Fig. 11. Laminar flame speeds of 50% CH_4 + 50% H_2 at 300 K and 1 atm in air; red symbols are experimental data, and red line is AramcoMech 1.3 predictions. The experimental data of Hu et al. [22] are also shown, together with AramcoMech 1.3 simulations as a black line. (For interpretation of the references to color in this figure legend, the reader is referred to the web version of this article.)

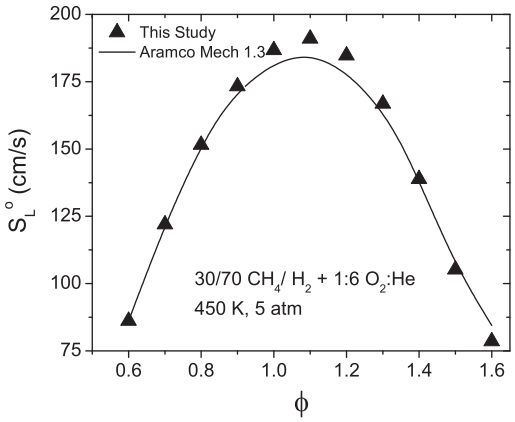

Fig. 12. Laminar flame speeds of 30% CH_4 + 70% H_2 at 5 atm and 450 K in 1:6 O_2:He; symbols are experimental data, and the line is the model prediction.

mixture of the two fuels. Figure 10 shows a comparison of the experimentally determined flame speeds between the pure fuel cases and the 50/50 blended case as measured in the present study, as well as numerical simulations of binary mixtures of the two fuels. It is readily seen that the blended-fuel flame speed portrays a non-linear relationship between the flame speed of its two pure components. Similar non-linear relationships have been found with fuel blending in another study by Kochar et al. [32]. Ilbas et al. [31] also show a plot of the flame speeds with the blend showing a non-linear profile that is closer to that of methane than hydrogen. This non-linear trend is indicative of the fact that the less-reactive component, methane, severely limits the flame speed even with an equal amount of the higher-reactive hydrogen component. Methane is usually flammable from equivalence ratios of 0.7–1.3, while the addition of hydrogen increases the flammability limit range from 0.5 to 1.4. The peak of the blended fuels falls much closer to that of methane and at a similar equivalence ratio. As the proportion of hydrogen increases, the peak flame speed moves towards richer mixtures and gets faster, and this behavior is observed experimentally to be strongly non-linear, Fig. 10. This behavior is also well-predicted by the model. Moreover, we have also included model predictions for 25/75, 10/90, 5/95 and 1/99 CH_4/H_2 blends in order to illustrate these clearly in the figure.

Figure 11 depicts the close up view of the 50/50 CH_4/H_2 blended experimental flame speed results. The solid lines represent the AramcoMech 1.3 predictions. The chemical kinetic model agrees very well with the experimental data. The peak flame speed occurs at $\phi = 1.1$, a similar equivalence ratio to that of methane. The profile of the flame speed curve is accurately predicted, and the model falls within the uncertainty band of the experimental data. Hu et al. [22] also performed experiments, which are included in Fig. 11. There is reasonable agreement between both data sets, given the error bars that are provided in the figure, but the present data are generally 5 cm/s slower than those measured by Hu et al. This difference cannot be explained by the slightly higher (3 K) temperature employed in the Hu et al. study, as the model predicts this difference to result in a 1 cm/s difference in flame speed near the peak values in the equivalence ratio range 0.8–1.2.

Figure 12 shows flame speed results for blending of much more hydrogen, 70%, than that of methane, 30%. These experiments were conducted at an elevated temperature and pressure, 450 K and 5 atm, respectively. The model agrees well with the experimental data for the fuel-lean and fuel-rich data, but under-predicts the measured peak flame speeds in the equivalence ratio range of 0.9–1.3 by approximately 8 cm/s at the peak of $\phi \approx 1.1$. The calculated uncertainty in the experimental measurements at this condition is the size of each data symbol. Overall, the model predictions prove to be accurate to well within 5%.

Shown in Fig. 13 are the flame speed results of 90% hydrogen with 10% methane at 450 K and 1 atm. The model agrees well with the experimental data for the fuel-lean data but under-predicts the measured peak flame speeds when the equivalence ratio reaches a value of 1.1 and then generally under-predicts the measured flame speeds by approximately 10 cm/s on the fuel-rich side. The peak is correctly predicted near $\phi = 1.4$, and the slope of the flame speed matches very well at lean and rich conditions. A sample uncertainty bar is shown that can explain the slightly higher profile than that of the model. Multiple data points are shown on this profile to show that these experiments are repeatable within the calculated uncertainty. Each of these mixtures was made directly in the combustion vessel; earlier studies have been conducted that show good agreement between experiments that were made previously in a mixing tank and allowed ample time to achieve homogeneity.

Finally, Fig. 14 shows the resultant flame speed from experiments conducted with 90% H_2 and 10% NG2 at an elevated pressure of 5 atm. As can be seen, the experimental data match the chemical kinetics model well. The model correctly predicts the peak flame speed at $\phi = 1.2$ while also matching the slope of the experimental

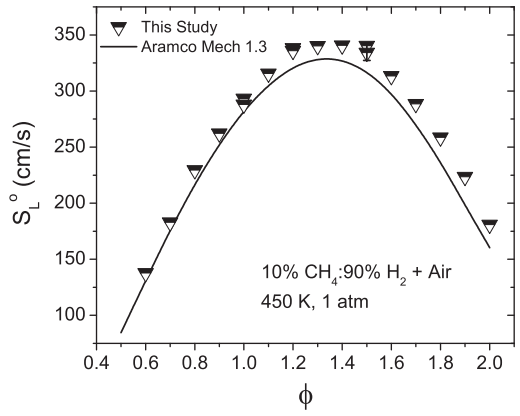

Fig. 13. Laminar flame speeds of 10% CH_4 + 90% H_2 at 1 atm and 450 K in air; symbols are experimental data, and the line is the model prediction.

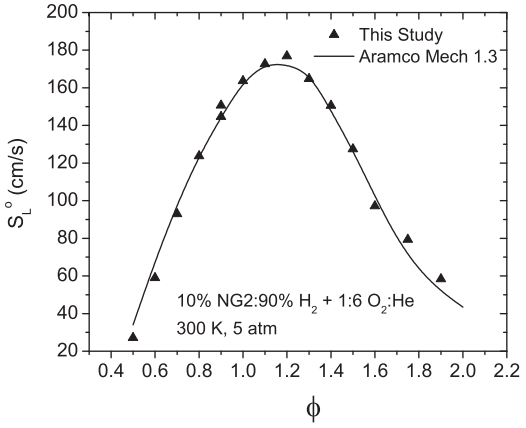

Fig. 14. Laminar flame speeds of 10% NG2 + 90% H_2 at 5 atm and 300 K in 1:6 O_2:He; symbols are experimental data, and the line is the model prediction.

data as conditions go to lean and rich. A sample uncertainty in flame speed is the size of the symbol in Fig. 14. With this uncertainty in mind, the model still over predicts the flame speed slightly. Specifically, the model noticeably over predicts at lean conditions (maximum of about 6%) while predicting very well at very rich conditions.

5. Mechanism validation

The chemical kinetic mechanism (AramcoMech 1.3) is also validated against recently available experimental data for methane/hydrogen blends by Zhang et al. [3]. In that study, ignition delay time measurements were taken behind reflected shock waves for methane/hydrogen mixtures at 5, 10, and 20 atm and an equivalence ratio of 0.5. In Fig. 15, the symbols represent the experimental data while the lines are model simulations. The solid lines correspond with AramcoMech 1.3, and the dotted lines represent GRI-Mech 3.0 [48]. Further comparisons of model predictions versus Zhang et al.'s experimental data are provided as Figs. 2 and 3 in the Supplementary material. For mixtures at 5, 10, and 20 atm, there is also a strong non-Arrhenius behavior exhibited by high hydrogen content mixtures. This is due to the competition between the main chain branching reaction $\dot{H} + O_2 = \ddot{O} + \dot{O}H$ and the propagation reaction, $\dot{H} + O_2(+M) = H\dot{O}_2(+M)$, which become more important at high pressures, please see Fig. 1 and relevant discussion in Kéromnès et al. [45].

The agreement between AramcoMech 1.3 and the experimental results is very good. The effect of hydrogen on methane ignition

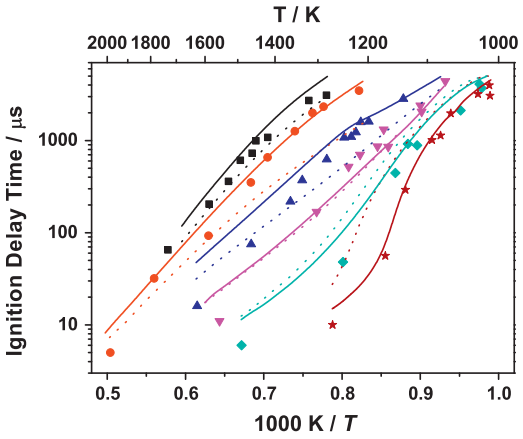

Fig. 15. Effect of hydrogen concentration on ignition delay times for CH_4/H_2 mixtures in a shock tube at 20 atm [3], ■ 100% CH_3, ● 80% CH_4/20% H_2, ▲ 60% CH_5/40% H_2, ▼ 40% CH_4/60% H_2, ♦ 20% CH_4/80% H_2, ★ 100% H_2. Solid lines are AramcoMech 1.3 predictions, dashed lines are GRI-Mech 3.0 predictions.

delay times is captured showing that the addition of even small amounts of hydrogen to methane leads to an increase in reactivity and shorter ignition delay times illustrating the promoting effect of hydrogen on the methane chemistry. Increasing the temperature also leads to shorter ignition times regardless of whether hydrogen or methane is controlling the reactivity. While modeling these experiments, a 4%/ms pressure rise due to the facility-dependent boundary layer was taken into account as described by the authors [3]. For all pressures and all conditions, AramcoMech 1.3 performs better than GRI-Mech 3.0, which does not accurately capture the effect of hydrogen addition. As mentioned previously, GRI-Mech 3.0 has a tendency to under-predict the reactivity of high hydrogen-containing fuels while over-predicting the reactivity of hydrocarbon fuels for ignition delays.

With regard to flame speeds from the literature, AramcoMech 1.3 is also shown to perform well compared with GRI-Mech 3.0_M for pure methane (Fig. 16) and pure hydrogen (Fig. 17). This result is due to the previously discussed differences in reactivity of the two mechanisms. However, Fig. 18 shows the large uncertainty in 80% methane/20% hydrogen laminar flame speeds at 1 atm and 298 K reported in the literature [15,62–64]. AramcoMech 1.3 and GRI-Mech 3.0_M both fall within this uncertainty and perform equally well. Overall, the mechanism has been revised to reflect the new data presented herein and performs well against these experiments and for both pure fuels and mixtures available in

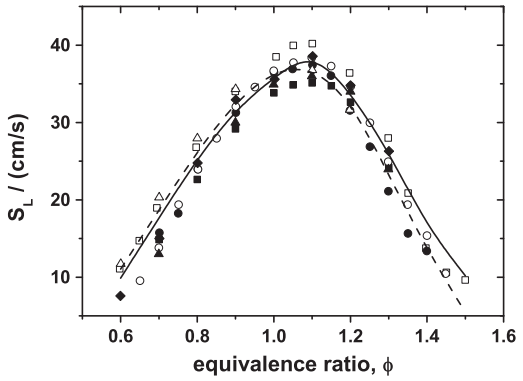

Fig. 16. Laminar flame speeds for 100% CH_4/air at 1 atm and 298 K, ■ Lowry et al. [36] □ Egolfopoulos et al. [50], • Vagelopoulos et al. [51], ○ Van Maaren et al. [52], ▲ Hassan et al. [17], △ Gu et al. [53], ◆ Rozenchan et al. [40], lines are model predictions.

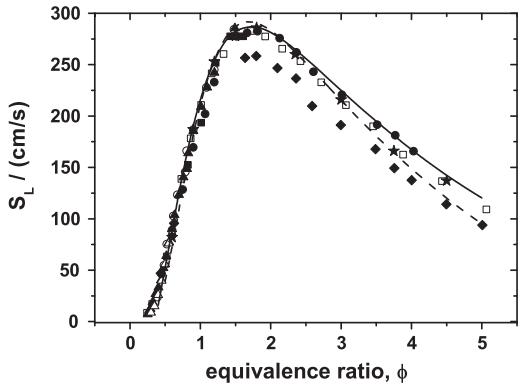

Fig. 17. Laminar flame speeds for 100% H_2 at 1 atm and 298 K in 'air', ■ Wu and Law [54] □ Dowdy et al. [55], • Tse et al. [56], ○ Law et al. [57], ▲ Egolfopoulos and Law [58], △ Vagelopoulos et al. [59], ♦ Aung et al. [60], ★ Kwon and Faeth [61], lines are model predictions.

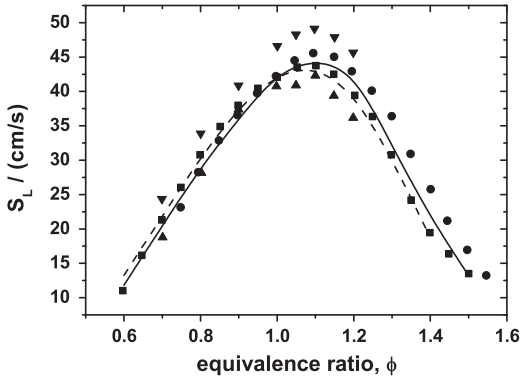

Fig. 18. Laminar flame speeds for 80% CH_4/20% H_2 at 1 atm and 298 K, ▼ Yu et al. [15], ■ Hermanns et al. [62], • Dirrenberger et al. [63], ▲ Halter et al. [64], lines are model predictions.

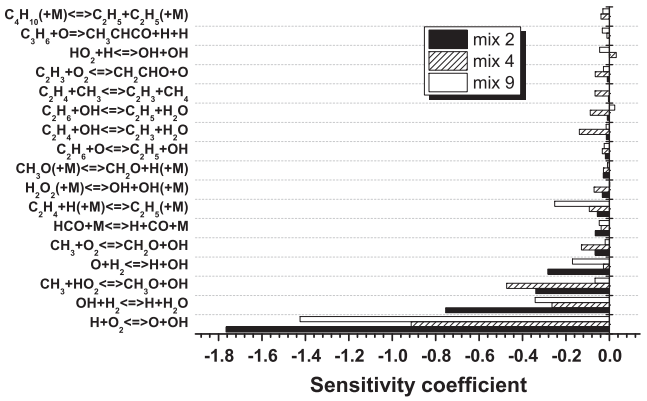

Fig. 19. Important reactions promoting reactivity to ignition delay times for mixtures 2 (60% H_2, 40% CH_4, ϕ = 0.5, 10 atm), 4 (30% H_2, 70% NG2, ϕ = 0.5, 30 atm), and 9 (80% H_2, 20% NG3, ϕ = 0.5, 1 atm) at 1250 K.

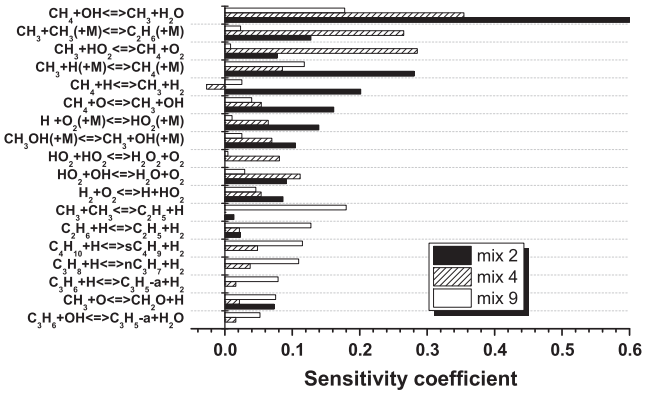

Fig. 20. Important reactions inhibiting reactivity to ignition delay times for mixtures 2 (60% H_2, ϕ = 0.5, 10 atm), 4 (30% H_2, ϕ = 0.5, 30 atm), and 9 (80% H_2, ϕ = 0.5, 1 atm) at 1250 K.

the literature [15,50–52,17,53,40,54–64]. Comparisons of model predictions compared to experimental data taken by Hermanns et al. [62] using the heat flux method are provided in Fig. 4 of the Supplementary material.

6. Sensitivity analysis

A sensitivity analysis was performed for ignition delay time mixtures 2, 4, and 9, all at an equivalence ratio of 0.5, and at a temperature of 1250 K. A brute force analysis was performed in which both the forward and reverse rate constants were separately increased and decreased by a factor of two using an automated code developed in-house, with sensitivities expressed using the formula:

$$S = \frac{\ln(\tau_+/\tau_-)}{\ln(k_+/k_-)} = \frac{\ln(\tau_+/\tau_-)}{\ln(2/0.5)}$$

A negative sensitivity coefficient is one in which the ignition delay time decreases and thus corresponds to an increase in reactivity, as shown in Fig. 19, contrarily a positive sensitivity coefficient corresponds to an increase in ignition delay time and thus a decrease in reactivity, as shown in Fig. 20.

These three mixtures were chosen due to their excellent agreement with the mechanism and wide spread of conditions, mix 2 comprising 40% CH_4 + 60% H_2 at 10 atm, mix 4 containing 30% H_2 + 70% NG2 at 30 atm, and mix 9 composed of 80% H_2 + 20% NG3 at 1 atm. As all the sensitivities were determined at the same equivalence ratio and temperature, similar reactions dominate the reaction kinetics controlling ignition delay time predictions, but these reactions have different relative sensitivities depending on the mixture composition. In general, mixtures 2 and 9 contain a higher hydrogen mole fraction relative to methane and thus hydrogen kinetics will tend to dominate, whereas in mix 4 there is a high concentration of hydrocarbons, and thus methyl radical chemistry will be of more importance than in mixtures 2 and 9. This effect of hydrocarbon/hydrogen split is reflected in the individual sensitivity analyses detailed below.

For all mixtures, the reaction most promoting reactivity is the high-temperature chain branching reaction $\dot{H} + O_2 = \ddot{O} + \dot{O}H$. This reaction is most important for high hydrogen-content mixtures 2 and 9 and lower pressures. Any reaction that depletes $(\dot{H} + O_2(+M) = H\dot{O}_2(+M))$ or increases $(H_2 + \dot{O}H = \dot{H} + H_2O)$ the hydrogen atom concentration will have either a positive or a negative sensitivity coefficient, respectively. At the conditions investigated, hydroperoxyl radical chemistry is important $(\dot{C}H_3 + H\dot{O}_2 = CH_3\dot{O} + \dot{O}H)$ due to the reaction $\dot{H} + O_2(+M) = H\dot{O}_2(+M)$. The $H\dot{O}_2$ radical so formed abstracts a hydrogen atom from another molecule to generate hydrogen peroxide $(RH + H\dot{O}_2 = \dot{R} + H_2O_2)$. This molecule decomposes to generate two hydroxyl $(\dot{O}H)$ radicals, $H_2O_2(+M) = \dot{O}H + \dot{O}H(+M)$. The reaction $H_2 + \ddot{O} = \dot{H} + \dot{O}H$ promotes reactivity as it produces a $\dot{H}$ atom (and an $\dot{O}H$ radical), but the reaction $CH_4 + \ddot{O} = \dot{C}H_3 + \dot{O}H$ inhibits reactivity as it produces relatively un-reactive methyl radicals (and an $\dot{O}H$ radical).

The most-inhibiting reaction for all mixtures is $CH_4 + \dot{O}H = \dot{C}H_3 + H_2O$, as this reaction competes with the promoting reaction

$H_2 + \dot{O}H = \dot{H} + H_2O$ for hydroxyl radicals, producing less-reactive methyl radicals compared to more-reactive hydrogen atoms. For mix 2, the recombination of a methyl radical with a hydrogen atom, $\dot{C}H_3 + \dot{H}(+M) = CH_4(+M)$, is the second most-inhibiting reaction, as it consumes two radicals and produces stable methane; another example is the reaction $\dot{C}H_3 + \dot{C}H_3(+M) = C_2H_6(+M)$. This reaction shows a higher sensitivity to mix 4 compared to mixtures 2 and 9, since mix 4 contains the highest concentration of methane. For mix 9, which contains the highest concentrations of larger hydrocarbons, ethyl radical chemistry shows some importance. The reactions of ethane, propane, and butane with a hydrogen atom all show positive sensitivity coefficients, reducing reactivity, as they compete with molecular oxygen for hydrogen atoms in the main chain-branching reaction $\dot{H} + O_2 = \ddot{O} + \dot{O}H$, which is highly promoting. The reaction $C_2H_6 + \dot{H} = \dot{C}_2H_5 + H_2$ and also the decomposition of the radicals produced by hydrogen atom abstraction for propane and butane also produce ethyl radicals. Ethyl radical decomposition to ethylene and a hydrogen atom promotes reactivity, as it produces a hydrogen atom but also generates ethylene which undergoes hydrogen-atom abstraction generating vinyl radicals which react with molecular oxygen, forming two radicals in a chain-branching process $\dot{C}_2H_3 + O_2 = \dot{C}H_2CHO + \ddot{O}$, Fig. 19.

Other reactions either promoting or reducing reactivity can be easily explained by the consumption of radical species generating stable molecules or by a competition between the formation of a hydrogen atom, which is promoting, or another radical such as methyl, which inhibits reactivity due to the overarching sensitivity of ignition delay times to the main chain branching reaction $\dot{H} + O_2 = \ddot{O} + \dot{O}H$ under these conditions.

7. Conclusions

New experimental data have been taken for natural gas/hydrogen blends over a wide range of conditions afforded by combining RCM, shock-tube, and laminar flame speed facilities into a single, cohesive study. Temperatures between 850 and 1800 K and pressures from 1 to 30 atm were studied for ignition delay times, and laminar flame speeds were obtained at 1 and 5 atm for initial temperatures of either 300 or 450 K. Hydrogen additions between 30% and 90% by volume of the fuel blend were covered in this paper. These new results were compared to the current AramcoMech 1.3 chemical kinetic mechanism developed at the NUIG research facility, and excellent agreement was observed. The experimental data show that ignition delay time decreases with increasing temperature, pressure, hydrogen fuel fraction, and increase in long-chain hydrocarbons. The current AramcoMech 1.3 mechanism was also validated against shock-tube ignition delay times and new flame speed data from the authors and laminar flame speed and ignition delay time data available in the literature. The agreement between the new shock-tube and RCM ignition delay time data is very good and is accurately captured by AramcoMech 1.3.

The mechanism accurately predicts the Zhang et al. [3] shock-tube ignition delay times except at the highest pressures for pure hydrogen. The new laminar flame speeds also provide good agreement with AramcoMech 1.3. One important observation with the laminar flame speed results for the H_2/NG2 and H_2/CH_4 data is that the addition of hydrogen has a nonlinear effect on flame speed. For example, at 50% H_2 addition, the blend's flame speed is much closer to that of pure methane than it is to pure hydrogen.

Overall, the agreement between the experimental data and AramcoMech 1.3 is quite good. For comparison, simulations with GRI-Mech 3.0 and GRI-Mech 3.0_M including the C_4 and C_5 NUIG sub-mechanisms have been performed. GRI-Mech 3.0 does not accurately describe the new ignition delay time experimental data, the new natural gas flame speeds and the Zhang et al. [3] shock-tube ignition delay times. However; it agrees well for the methane/hydrogen flame speeds. This agreement is possibly due to the tendency of GRI 3.0 to under-predict hydrogen reactivity and over-predict hydrocarbon reactivity compared to AramcoMech 1.3. Nevertheless, there is a large uncertainty in the literature for laminar flame speeds taken at the same conditions, and both mechanisms fall within this uncertainty. We believe that this work offers an important contribution to the gas turbine industry. AramcoMech 1.3 has been shown to predict accurate results for natural gas/hydrogen mixtures and might be used to precisely validate other natural gas experimental data at gas turbine relevant conditions.

Acknowledgments

This work was supported by Science Foundation Ireland under Grant No. [08/IN1./I2055]. We also acknowledge the support of Alstom Power Ltd. A. Morones was supported by CONANCYT of Mexico and CIDESI, and M. Davis was supported in part by a Graduate Diversity Fellowship from Texas A&M University.

Appendix A. Supplementary material

Supplementary data associated with this article can be found, in the online version, at http://dx.doi.org/10.1016/j.combustflame.2013.12.005.

References

[1] M. Brower, E.L. Petersen, W. Metcalfe, H.J. Curran, M. Füri, G. Bourque, N. Aluri, F. Güthe, J. Eng. Gas. Turb. Power 135 (2013) (Article No. 21504).
[2] F. Ma, M. Wang, L. Jiang, J. Deng, R. Chen, N. Naeve, S. Zhao, Int. J. Hydrogen Energy 35 (2010) 12502–12509.
[3] Y. Zhang, Z. Huang, L. Wei, J. Zhang, C.K. Law, Combust. Flame 159 (2012) 918–931.
[4] N. Donato, C. Aul, E. Petersen, C. Zinner, H. Curran, G. Bourque, J. Eng. Gas. Turb. Power 132 (2010) (Article No. 051502).
[5] D. Healy, N.S. Donato, C.J. Aul, E.L. Petersen, C.M. Zinner, G. Bourque, H.J. Curran, Combust. Flame 157 (2010) 1526–1539.
[6] D. Healy, N.S. Donato, C.J. Aul, E.L. Petersen, C.M. Zinner, G. Bourque, H.J. Curran, Combust. Flame 157 (2010) 1540–1551.
[7] D. Healy, M.M. Kopp, N.L. Polley, E.L. Petersen, G. Bourque, H.J. Curran, Energy Fuels 24 (2010) 1617–1627.
[8] D. Healy, D.M. Kalitan, C.J. Aul, E.L. Petersen, G. Bourque, H.J. Curran, Energy Fuels 24 (2010) 1521–1528.
[9] D. Healy, Experimental and Modelling Studies of Natural Gas Mixtures in a Rapid Compression Machine, Ph. D. Thesis, National University of Ireland, Galway, 2009.
[10] O. Park, P.S. Veloo, N. Liu, F.N. Egolfopoulos, Proc. Combust. Inst. 33 (2011) 887–894.
[11] S. Gersen, N.B. Anikin, A.V. Mokhov, H.B. Levinsky, Int. J. Hydrogen Energy 33 (2008) 1957–1964.
[12] S. Gersen, H. Darmeveil, H. Levinsky, Combust. Flame 159 (2012) 3472–3475.
[13] R. Crossley, E. Dorko, K. Scheller, A. Burcat, Combust. Flame 19 (1972) 373–378.
[14] J. de Vries, E.L. Petersen, Proc. Combust. Inst. 31 (2007) 3163–3171.
[15] G. Yu, C. Law, C. Wu, Combust. Flame 63 (1986) 339–347.
[16] Z. Huang, Y. Zhang, K. Zeng, B. Liu, Q. Wang, D. Jiang, Combust. Flame 146 (2006) 302–311.
[17] M. Hassan, K. Aung, G. Faeth, Combust. Flame 115 (1998) 539–550.
[18] K. Aung, L. Tseng, M. Ismail, G. Faeth, Combust. Flame 102 (1995) 526–530.
[19] Z. Chen, P. Dai, S. Chen, Int. J. Hydrogen Energy 37 (2012) 10390–10396.
[20] F. Wu, A. Kelley, C. Tang, D. Zhu, C. Law, Int. J. Hydrogen Energy 36 (2011) 13171–13180.
[21] C. Tang, Z. Huang, C. Law, Proc. Combust. Inst. 33 (2011) 921–928.
[22] E. Hu, Z. Huang, J. He, C. Jin, J. Zheng, Int. J. Hydrogen Energy 34 (2009) 4876–4888.
[23] L. Brett, J. MacNamara, P. Musch, J. Simmie, Combust. Flame 124 (2001) 326–329.
[24] S.M. Gallagher, H.J. Curran, W.K. Metcalfe, D. Healy, J.M. Simmie, G. Bourque, Combust. Flame 153 (2008) 316–333.
[25] Chemkin Pro 15101, Reaction Design: San Diego, 2010.
[26] G. Mittal, A. Bhari, Combust. Flame 160 (2013) 2975–2981.
[27] C. Aul, An Experimental Study into the Ignition of Methane and Ethane Blends in a New Shock-Tube Facility, M.S. Thesis, Texas A&M University, College Station, TX, 2009.

[28] C.J. Aul, W.K. Metcalfe, S.M. Burke, H.J. Curran, E.L. Petersen, Combust. Flame 160 (2013) 1153–1167.
[29] E.L. Petersen, M.J.A. Rickard, M.W. Crofton, E.D.A. Abbey, M.J. Traum, D.M. Kalitan, Meas. Sci. Technol. 16 (2005) 1716–1729.
[30] E.L. Petersen, Combust. Sci. Technol. 181 (2009) 1123–1144.
[31] M. Ilbas, A. Crayford, I. Yilmaz, P. Bowen, N. Syred, Int. J. Hydrogen Energy 31 (2006) 1768–1779.
[32] Y. Kochar, J. Seitzman, T. Lieuwen, W. Metcalfe, S. Burke, H. Curran, M. Krejci, W. Lowry, E. Petersen, Laminar flame speed measurements and modeling of alkane blends at elevated pressures with various diluents, in: 2011 ASME Turbo Expo, Vancouver, Canada, June 6–10, 2011, Paper GT2011-45122.
[33] P. Ross, McGraw-Hill, 1996.
[34] G. Bourque, D. Healy, H. Curran, C. Zinner, D. Kalitan, J. de Vries, C. Aul, E. Petersen, J. Eng. Gas Turb. Power 132 (2010) 021504.
[35] J. de Vries, A Study on Spherical Expanding Flame Speeds of Methane, Ethane, and Methane/Ethane Mixtures at Elevated Pressures, Ph.D. thesis, Texas A&M University, 2009.
[36] W. Lowry, J. de Vries, M. Krejci, E. Petersen, Z. Serinyel, W. Metcalfe, H. Curran, G. Bourque, J. Eng. Gas Turb. Power 133 (2011) 091501–091509.
[37] M.C. Krejci, Development of a New Flame Speed Vessel to Measure the Effect of Steam Dilution on Laminar Flame Speeds of Syngas Fuel Blends at Elevated Pressures and Temperatures, Ph.D. Thesis, Texas A&M University, 2012.
[38] M. Krejci, O. Mathieu, A.J. Vissotski, S. Ravi, T.G. Sikes, E.L. Petersen, A. Kéromnès, W. Metcalfe, H.J. Curran, J. Eng. Gas Turb. Power 135 (2013) 021503–021509.
[39] D. Plichta, E. Petersen, S. Burke, H. Curran, Laminar flame speeds of hydrocarbons with helium dilution at raised pressures and temperatures, in: AIAA Paper 2013-1164.
[40] G. Rozenchan, D. Zhu, C. Law, S. Tse, Proc. Combust. Inst. 29 (2002) 1461–1470.
[41] Z. Chen, Combust. Flame 158 (2011) 291–300.
[42] S. Kline, F. McClintock, Mech. Eng. (1953) 3–8.
[43] M. Elia, M. Ulinski, M. Metghalchi, ASME Trans. 123 (2001) 90–96.
[44] W.K. Metcalfe, S.M. Burke, S.S. Ahmed, H.J. Curran, Int. J. Chem. Kinet. 45 (2013) 638–675.
[45] A. Kéromnès, W.K. Metcalfe, K.A. Heufer, N. Donohoe, A.K. Das, C.-J. Sung, J. Herzler, C. Naumann, P. Griebel, O. Mathieu, M.C. Krejci, E.L. Petersen, W.J. Pitz, H.J. Curran, Combust. Flame 160 (2013) 995–1011.
[46] A. Laskin, H. Wang, C. Law, Int. J. Chem. Kinet. 32 (2000) 589–614.
[47] S. Davis, C. Law, H. Wang, Combust. Flame 119 (1999) 375–399.
[48] G. Smith, D.M. Golden, M. Frenklach, N. Moriarty, B. Eiteneer, M. Goldenberg, C. Bowman, R. Hanson, S. Song, W. Gardiner, Jr., V. Lissianski, Z. Qin, 1999. <www.me.berkeley.edu/grimech/>.
[49] G. Mittal, C.J. Sung, M. Fairweather, A.S. Tomlin, J.F. Griffiths, K.J. Hughes, Proc. Combust. Inst. 31 (2009) 419–427.
[50] F. Egolfopoulos, P. Cho, C. Law, Combust. Flame 76 (1989) 375–391.
[51] C. Vagelopoulos, F. Egolfopoulos, Proc. Combust. Inst. 26 (1998) 513–519.
[52] A. van Maaren, D.S. Thung, L.R.H. De Goey, Combust. Sci. Technol. 96 (1994) 327–344.
[53] X. Gu, M. Haq, M. Lawes, R. Woolley, Combust. Flame 121 (2000) 41–58.
[54] C. Wu, C. Law, Proc. Combust. Inst. 20 (1985) 1941–1949.
[55] D.R. Dowdy, D. Smith, S. Taylor, A. Williams, Proc. Combust. Inst. 23 (1991) 325–332.
[56] S. Tse, D. Zhu, C. Law, Proc. Combust. Inst. 28 (2000) 1793–1800.
[57] H. Chelliah, K. Seshadri, C. Law, in: N. Peters, B. Rogg (Eds.), Reduced Kinetic Mechanisms for Applications in Combustion Systems, Lecture Notes in Physics Monographs, vol. 15, Springer, Berlin, Heidelberg, 1993, pp. 224–240.
[58] F. Egolfopoulos, C. Law, Proc. Combust. Inst. 23 (1991) 333–340.
[59] C. Vagelopoulos, F. Egolfopoulos, C. Law, Proc. Combust. Inst. 25 (1994) 134–1347.
[60] K. Aung, M. Hassan, G. Faeth, Combust. Flame 109 (1997) 1–24.
[61] O. Kwon, G. Faeth, Combust. Flame 124 (2001) 590–610.
[62] R.T.E. Hermanns, A.A. Konnov, R.J.M. Bastiaans, L.P.H. de Goey, K. Lucka, H. Koehne, Fuel 89 (2010) 114–121.
[63] P. Dirrenberger, H. Le Gall, R. Bounaceur, O. Herbinet, P.-A. Glaude, A. Konnov, F. Battin-Leclerc, Energy Fuels 25 (2011) 3875–3884.
[64] F. Halter, C. Chauveau, N. Djeballi-Chaumeix, I. Gokalp, Proc. Combust. Inst. 30 (2005) 201–208.